Computational Efficiency Improvement for Analyzing Bending and Tensile Behavior of Woven Fabric Using Strain Smoothing Method

Q. T. Nguyen[1(✉)], A. J. P. Gomes[2], and F. N. Ferreira[1]

[1] School of Engineering, Centre for Textile Science and Technology, University of Minho, Campus de Azurém, 4800-058 Guimarães, Portugal
quyenum@gmail.com

[2] Faculty of Engineering, Institute of Telecommunications, University of Beira Interior, R. Marquês de Ávila e Bolama, 6201-001 Covilhã, Portugal

Abstract. The tensile and bending behavior of woven fabrics are among the most important characteristics in complex deformation analysis and modelling of textile fabrics and they govern many aesthetics and performance aspects such as wrinkle/buckle, hand and drape. In this paper, a numerical method for analyzing of the tensile and bending behavior of plain-woven fabric structure was developed. The formulated model is based on the first-order shear deformation theory (FSDT) for a four-node quadrilateral element (Q4) and a strain smoothing method in finite elements, referred as a cell-based smoothed finite element method (CS-FEM). The physical and low-stress mechanical parameters of the fabric were obtained through the fabric objective measurement technology (FOM) using the Kawabata evaluation system for fabrics (KES-FB). The results show that the applied numerical method provides higher efficiency in computation in terms of central processing unit (CPU) time than the conventional finite element method (FEM) because the evaluation of compatible strain fields of Q4 element in CS-FEM model is constants, and it was also appropriated for numerical modelling and simulation of mechanical deformation behavior such as tensile and bending of woven fabric.

Keywords: Plain woven fabric structure · Fabric objective measurement
First-order shear deformation theory
Cell-based smoothed finite element method

1 Introduction

In engineering sectors of textile and apparel industry, numerical modelling and simulation have been widely developed and applied in solving complex problems in the product design and engineering process to predict how an apparel product reacts to real-world forces, moisture absorption, heat transfer and other physical effects and so forth [1–4]. Tensile properties are considered as the most important factor that govern the performance characteristics of textile fabrics. The investigation of tensile properties

O. Gervasi et al. (Eds.): ICCSA 2018, LNCS 10960, pp. 138–148, 2018.
https://doi.org/10.1007/978-3-319-95162-1_10

encounters many difficulties due to the complexity of fabric structure leading to variation strain during deformation [5]. In general, each fabric sheet consists of a large amount of constituent fibers and yarns which will response subsequently to a series of complex movements under any deformation state. This makes the mechanical properties of textile fabrics more complicated due to both fibers and yarns behaving in a non-Hookean law during deformation and presenting hysteresis effect [5, 6]. In addition, mechanical bending properties of textile fabrics govern many aspects of fabric appearance and performance, such as wrinkle/buckle, hand and drape. These are one of the most important characteristics in complex deformation analysis and modelling of textile fabrics.

Numerical modelling of large-deflection elastic structural mechanics from numerical models have been widely applied to examine specific textile fabric engineering and apparel industry problems [6]. The applicability of mechanical modelling of tensile and bending behavior of textile fabrics is very limited because it requires a large number of mechanical parameters and is, therefore, difficult to express in a closed form [3]. The most detailed analysis of the bending behavior of plain-woven fabrics can be found in [7] The tensile and bending properties of woven fabrics have, therefore, received considerable attention in both literature and model experiments.

A strain smoothing operation [8] was proposed recently as a CS-FEM A cell-based strain smoothing method in finite elements (CS-FEM), was improved the accuracy and convergence rate of the existing conventional finite element finite element method (FEM) of elastic solid mechanics problems [9–12]. It was also applied to improve formulation of a locking-free four-node quadrilateral flat shell element (Q4) with five degrees of freedom per node, and able to reduce the mesh distortion sensitivity and enhance the coarse mesh accuracy.

Therefore, this paper presents a numerical solution that offer a better efficiency of computation but effective performance in modelling and simulation of tensile and bending behavior of woven fabric structures. The numerical model is based on the integration scheme of CS-FEM model into the Mindlin-Reissner plate element and the plane-stress element using a four-node quadrilateral element [13–15]. The plain-woven fabric is assumed as an elastic with orthotropic anisotropy for which the constitutive laws formulated are using low-stress mechanical properties obtained from KES-FB [6]. The numerical result is subjected to evaluate and investigate the applicability of CS-FEM models using one smoothing cell to improve the computational efficiency in analyzing the bending and tensile behavior of woven fabric.

2 Formulations of the Shell Structure

Consider a reference plane that occupies a domain $\Omega \in R^3$ bounded by Γ at the middle surface of shell is. Let u, v and w be the translational displacements and transverse displacement, θ_x and θ_y be the rotations in the xz and yz planes in the Cartesian coordinate system as shown in Fig. 1.

The problem domain Ω is discretized into a set of four-node quadrilateral flat shell elements Ω^e with boundary Γ^e. The generalized displacement vector $\boldsymbol{u}^h$ can be then approximated as

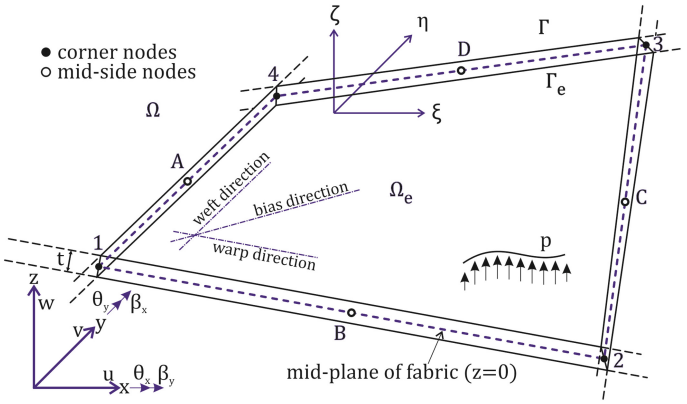

Fig. 1. A four-node quadrilateral flat shell element

$$\boldsymbol{u}^h = \sum_{I=1}^{4} \begin{bmatrix} N_I & 0 & 0 & 0 & 0 \\ 0 & N_I & 0 & 0 & 0 \\ 0 & 0 & N_I & 0 & 0 \\ 0 & 0 & 0 & 0 & N_I \\ 0 & 0 & 0 & N_I & 0 \end{bmatrix} \boldsymbol{q}_I, \tag{1}$$

in which N_I is shape function and $\boldsymbol{q}_I^T = \{ u_I \quad v_I \quad w_I \quad \theta_{xI} \quad \theta_{yI} \}$ is vector of nodal degrees of freedom associated with each of nodes I.

Based on the FSDT, the generalized strains comprises of three parts, namely $\boldsymbol{\varepsilon}^m$, $\boldsymbol{\varepsilon}^b$ and $\boldsymbol{\varepsilon}^s$. The membrane strain $\boldsymbol{\varepsilon}^m$, curvature strain $\boldsymbol{\varepsilon}^b$ and transverse shear strain $\boldsymbol{\varepsilon}^s$ are defined, respectively, as

$$\boldsymbol{\varepsilon}^{\boldsymbol{m}} = \begin{Bmatrix} \frac{\partial u}{\partial x} \\ \frac{\partial v}{\partial y} \\ \frac{\partial u}{\partial y} + \frac{\partial v}{\partial y} \end{Bmatrix} = \sum_{I=1}^{4} \begin{bmatrix} N_{I,x} & 0 & 0 & 0 & 0 \\ 0 & N_{I,y} & 0 & 0 & 0 \\ N_{I,y} & N_{I,x} & 0 & 0 & 0 \end{bmatrix} \boldsymbol{q}_I = \boldsymbol{B}^m \boldsymbol{q}, \tag{2}$$

$$\boldsymbol{\varepsilon}^b = \begin{Bmatrix} \frac{\partial \theta_x}{\partial x} \\ \frac{\partial \theta_y}{\partial y} \\ \frac{\partial \theta_y}{\partial y} - \frac{\partial \theta_x}{\partial y} \end{Bmatrix} = \sum_{I=1}^{4} \begin{bmatrix} 0 & 0 & 0 & N_{I,x} & 0 \\ 0 & 0 & -N_{I,y} & 0 & 0 \\ 0 & 0 & -N_{I,x} & N_{I,y} & 0 \end{bmatrix} \boldsymbol{q}_I = \boldsymbol{B}^b \boldsymbol{q}, \tag{3}$$

$$\boldsymbol{\varepsilon}^s = \begin{Bmatrix} \frac{\partial \mathrm{W}}{\partial x} + \theta_y \\ \frac{\partial \mathrm{W}}{\partial y} - \theta_x \end{Bmatrix} = \sum_{I=1}^{4} \begin{bmatrix} 0 & 0 & N_{I,x} & 0 & N_I \\ 0 & 0 & N_{I,y} & -N_I & 0 \end{bmatrix} \boldsymbol{q}_I = \boldsymbol{B}^s \boldsymbol{q}, \tag{4}$$

where superscripts *m, b* and *s* stand for the membrane, bending (curvature) and transverse shear elements, respectively, and $\boldsymbol{B}$ is the strain matrices.

The constitutive relations between the stress and train fields of elements are defined as

$$\boldsymbol{\sigma}^m = \{\, \sigma_x \quad \sigma_y \quad \tau_{xy} \,\}^T = \boldsymbol{D}^m \boldsymbol{\varepsilon}^m, \tag{5}$$

$$\boldsymbol{\sigma}^b = \{\, \sigma_x \quad \sigma_y \quad \tau_{xz} \,\}^T = \boldsymbol{D}^b \boldsymbol{\varepsilon}^b, \tag{6}$$

$$\boldsymbol{\sigma}^s = \{\, \tau_{xz} \quad \tau_{yz} \,\}^T = \boldsymbol{D}^s \boldsymbol{\varepsilon}^s, \tag{7}$$

in which the stress components σ_x and σ_y, shear components γ_{xy}, τ_{xy}, τ_{xz} and τ_{yz} lead to the force and moment resultants per unit length. Let subscripts 1 and 2 be associated with directions of the warp and weft yarns, and h, E, v, B, H and G are respectively the thickness of shell, Young's modulus, Poisson's ratios, flexural moduli, torsional rigidity and shear modulus. Then the material matrices related to the plane-stress $\boldsymbol{D}^m$, bending $\boldsymbol{D}^b$ and transverse shear deformation $\boldsymbol{D}^s$ are defined, respectively, as

$$\begin{gathered} D^m = \int_{\frac{h}{2}}^{\frac{h}{2}} \begin{bmatrix} \frac{E_1}{1-v_1 v_2} & \frac{v_2 E_1}{1-v_2 v_1} & 0 \\ \frac{v_1 E_2}{1-v_1 v_2} & \frac{E_2}{1-v_2 v_1} & 0 \\ 0 & 0 & G \end{bmatrix} dz, \\ D^b = \int_{\frac{h}{2}}^{\frac{h}{2}} z^2 \begin{bmatrix} B_1 & 0 & 0 \\ 0 & B_2 & 0 \\ 0 & 0 & H \end{bmatrix} dz,\ D^s = \int_{\frac{h}{2}}^{\frac{h}{2}} \frac{5}{6} G \begin{bmatrix} 1 & 0 \\ 0 & 1 \end{bmatrix} dz, \end{gathered} \tag{8}$$

The discretized system equations in term of a weak form solution of generalized displacement field $\boldsymbol{u}^h$ that satisfies the Galerkin weak form for the tensile and bending problems can be written as

$$\boldsymbol{K}\boldsymbol{q} = \boldsymbol{f}, \tag{9}$$

in which $\boldsymbol{f}$ indicates the force vector and $\boldsymbol{K} = \boldsymbol{K}^m + \boldsymbol{K}^b + \boldsymbol{K}^s$ is the global stiffness matrix [16].

3 Cell-Base Strain Smoothing Operation

The cell-based strain smoothing operation [17, 18] performs over the kth smoothing domain Ω_k^s with Γ_k^s of the element Ω^e is addressed as

$$\bar{\nabla}\boldsymbol{u}(\mathrm{x}_k) = \int_{\Omega_i^s} \boldsymbol{\varepsilon}(\mathrm{x}) \Phi(\mathrm{x} - \mathrm{x}_k) d\Omega, \tag{10}$$

where Φ is a smoothing or weight function associated with point x_i in Ω_k^s, and $\nabla\boldsymbol{u}(\mathrm{x}) \cong \boldsymbol{\varepsilon}(\mathrm{x})$. This smoothing function must satisfy the basic conditions of $\Phi \geq 0$ and $\int_{\Omega_i^s} \Phi d\Omega = 1$. For simplicity, a piecewise constant function is applied here, as given by:

$$\Phi(\mathrm{x} - \mathrm{x}_k) = \begin{cases} 1/A_k^s, & \mathrm{x} \in \Omega_k^s \\ 0, & \mathrm{x} \notin \Omega_k^s \end{cases}, \tag{11}$$

where $A_k^s = \int_{\Omega_k^s} d\Omega$ the area of the kth smoothing domain $\Omega_k^s \subset \Omega^e$.

In an CS-FEM model, the strain in smoothing domain Ω_k^s can be further assumed to be a constant and equals $\bar{\boldsymbol{\varepsilon}}(\mathrm{x}_k)$. By substituting smoothing function Φ into Eq. (10), the averaged/smoothed gradient of displacement is defined as

$$\bar{\boldsymbol{\varepsilon}}_k = \bar{\boldsymbol{\varepsilon}}(\mathrm{x}_k) = \frac{1}{A_k^s} \int_{\Omega_k^s} \boldsymbol{\varepsilon}(\mathrm{x}) d\Omega = \frac{1}{A_k^s} \int_{\Gamma_k^s} \boldsymbol{n}(\mathrm{x}) \cdot \boldsymbol{u}(\mathrm{x}) d\Gamma. \tag{12}$$

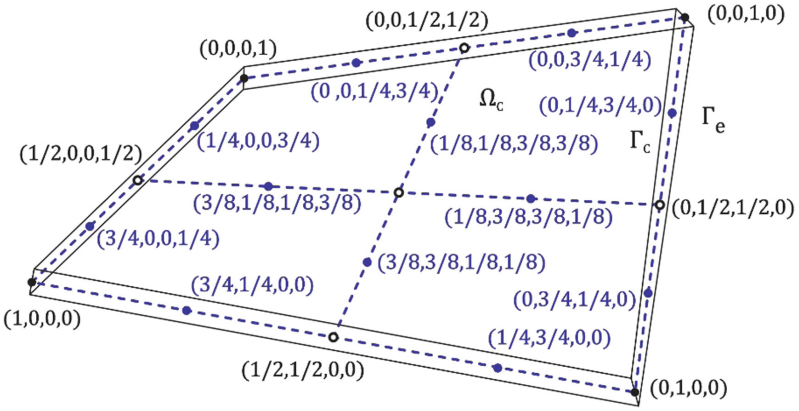

Fig. 2. An discretized element of domain is further divided into 1-, 2-, 3- and 4 smoothing domains (SDs) including the orthogonal nodal shape functions N_I.

The averaged/smoothing strain operation for membrane strains and curvature strains in Eqs. (2) and (3), as shown in Fig. 2, can be reformed as

$$\boldsymbol{\varepsilon}^m(\mathrm{x}_k) = \frac{1}{A_k^s} \int_{\Omega_k^s} \boldsymbol{\varepsilon}^m(\mathrm{x}_k) d\Omega = \frac{1}{A_k^s} \int_{\Gamma_k^s} \boldsymbol{n} \cdot \boldsymbol{u}(\mathrm{x}_k) d\Gamma = \sum_{I=1}^{4} \boldsymbol{B}_{kI}^m(\mathrm{x}_k) \cdot \boldsymbol{q}_I^m, \tag{13}$$

$$\boldsymbol{\varepsilon}^b(\mathrm{x}_k) = \frac{1}{A_k^s} \int_{\Omega_k^s} \boldsymbol{\varepsilon}^b(\mathrm{x}_k) d\Omega = \frac{1}{A_k^s} \int_{\Gamma_k^s} \boldsymbol{n} \cdot \boldsymbol{u}(\mathrm{x}_k) d\Gamma = \sum_{I=1}^{4} \boldsymbol{B}_{kI}^b(\mathrm{x}_k) \cdot \boldsymbol{q}_I^p, \tag{14}$$

in which $\boldsymbol{n}$ is the outward normal matrix containing the components of the outward unit normal vector to the boundary Γ_k^s and $\boldsymbol{B}_{kI}$ stand for the smoothed gradient matrices defined as

$$\boldsymbol{B}_{kI}^m(\mathrm{x}_k) = \begin{bmatrix} \bar{b}_{kIx} & 0 & 0 & 0 & 0 \\ 0 & \bar{b}_{kIy} & 0 & 0 & 0 \\ \bar{b}_{kIy} & \bar{b}_{kIx} & 0 & 0 & 0 \end{bmatrix}, \boldsymbol{B}_{kI}^b(\mathrm{x}_k) = \begin{bmatrix} 0 & 0 & 0 & \bar{b}_{kIx} & 0 \\ 0 & 0 & -\bar{b}_{kIy} & 0 & 0 \\ 0 & 0 & -\bar{b}_{kIx} & \bar{b}_{kIy} & 0 \end{bmatrix}, \tag{15}$$

where

$$\bar{b}_{kIx} = \frac{1}{A_k^s} \int_{\Gamma_k^s} n_x N_I d\Gamma = \frac{1}{A_k^s} \sum_{b=1}^{n_b^s} n_{xb} N_I\left(\mathrm{x}_b^G\right) l_b,$$
$$\bar{b}_{kIy} = \frac{1}{A_k^s} \int_{\Gamma_{k,c}^e} n_y N_I d\Gamma = \frac{1}{A_k^s} \sum_{b=1}^{n_b^s} n_{yb} N_I\left(\mathrm{x}_b^G\right) l_b. \tag{16}$$

In Eq. (16), n_{xb} and n_{yb} indicate the components of the outward unit normal to the bth boundary segment and x_b^G is the cooinate value of Gauss point of the bth boundary segment. Using Eq. (15), the membrane and bending terms of the stiffness matrix $\boldsymbol{K}^m$ and $\boldsymbol{K}^b$ in Eq. (9) can be evaluated using 1 to 4 smoothing cells.

4 Mixed Interpolation of Tensorial Components

Mindlin-Reissner (or FSDT) plate elements exhibit a shear locking phenomenon due to incorrect transverse forces under bending, or in the case of the thickness of the plate tends to zero. To overcome the shear locking phenomena, the approximation of the shear strain fields $\boldsymbol{\gamma}$ is formulated with the mixed interpolation of tensorial components approaches [13] as

$$\boldsymbol{\varepsilon}^s = \begin{Bmatrix} \gamma_{xz} \\ \gamma_{yz} \end{Bmatrix} = \boldsymbol{J}^{-1} \frac{1}{2} \begin{Bmatrix} (1-\eta)\gamma_\xi^B + (1+\eta)\gamma_\xi^D \\ (1-\xi)\gamma_\eta^A + (1+\xi)\gamma_\eta^C \end{Bmatrix}, \tag{17}$$

in which

$$\begin{Bmatrix} \gamma_\xi \\ \gamma_\eta \end{Bmatrix} = \frac{1}{2} \begin{Bmatrix} (1-\eta)\gamma_\xi^B + (1-\eta)\gamma_\xi^D \\ (1-\xi)\gamma_\eta^A + (1-\xi)\gamma_\eta^C \end{Bmatrix}, \tag{18}$$

and $\boldsymbol{J}$ is Jacobian transformation matrix and superscripts A, B, C and D are the mid-side node, as shown in Fig. 1. Expressing $\gamma_\eta^A, \gamma_\eta^C$ and $\gamma_\xi^B, \gamma_\xi^D$ in terms of the discretized fields $\boldsymbol{q}_I$, the shear part of the stiffness matrix is then rewritten as

$$\boldsymbol{B}_I^s = \mathbf{J}^{-1} \begin{bmatrix} 0 & 0 & \frac{\partial N_I}{\partial \xi} & \xi_i \frac{\partial x^M}{\partial \xi} \frac{\partial N_I}{\partial \xi} & \xi_i \frac{\partial y^M}{\partial \xi} \frac{\partial N_I}{\partial \xi} \\ 0 & 0 & \frac{\partial N_I}{\partial \eta} & \eta_i \frac{\partial x^L}{\partial \eta} \frac{\partial N_I}{\partial \eta} & \eta_i \frac{\partial y^L}{\partial \eta} \frac{\partial N_I}{\partial \eta} \end{bmatrix}. \tag{19}$$

The coordinates of the unit square are $\xi_i \in \{-1,\ 1,\ 1,\ -1\}$ and $\eta_i \in \{-1,\ -1,\ 1,\ 1\}$ and the allocation of the mid-side nodes to the corner nodes of element are given as $(i; M; L) \in \{(1; B; A); (2; B; C); (3; D; C); (4; D; A)\}$. Using Eq. (19), the shear term of the stiffness matrix $\boldsymbol{K}^s$ in Eq. (9) can be evaluated using full integration of 2×2 Gauss Quadrature.

5 Numerical Implementation and Results

The numerical results of a four-node quadrilateral flat shell element (Q4) for bending and tensile analysis of a square woven fabric sheet having boundaries include clamped edges (C), simply supported edges (S) and free edges (F) under uniform pressure was implemented for both FEM and CS-FEM models, see Figs. 3 and 4.

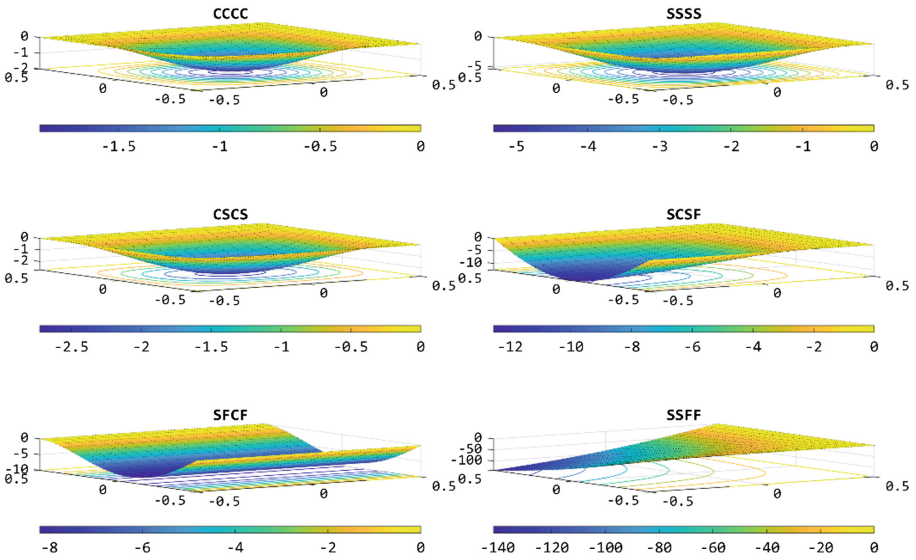

Fig. 3. Bending deformation of a plain-woven fabric sheet, using 20 × 20 Q4 elements and one smoothing cell per element with different boundaries.

Mechanical and physical parameters of a plain-woven fabric sample were computed with KES-FB comprising of the thickness [mm] of $h = 0.0848$, elastic modulus [gf/cm], $E_1 = 3823.7993$, $E_2 = 14092.4464$ and $E_{12} = 6896.5517$, Poisson's ratio $v_1 = 0.0211$ and $v_2 = 0.0778$, bending rigidity $[gf.cm^2/cm]$ of $B_1 = 0.1237$, $B_2 = 0.1333$ and $B_{12} = 0.0880$, transverse shear modulus [gf.cm^2] of $G = 217.3100$.

The computational results for tensile behavior, as illustrated in Figs. 5 and 6, produced an accurate numerical results implemented by one smoothing cell per a four-node quadrilateral shell element and it was compared with the conventional FEM's results, which is clearly well-balanced feature of the CS-FEM.

The numerical results also indicated that the membrane elements implemented by CS-FEM are well refined, not distorted and not coarse even. Thus, the strain smoothing operation for four-node flat shell element are in good agreement with the conventional FEM solution.

In order to compare the accuracy of strain fields evaluated by CS-FEM and FEM, train fields of membrane and curvature of the formulated shell element was implemented using Eqs. (2) and (3) for FEM and Eq. (15) for CS-FEM. Figure 7 indicates

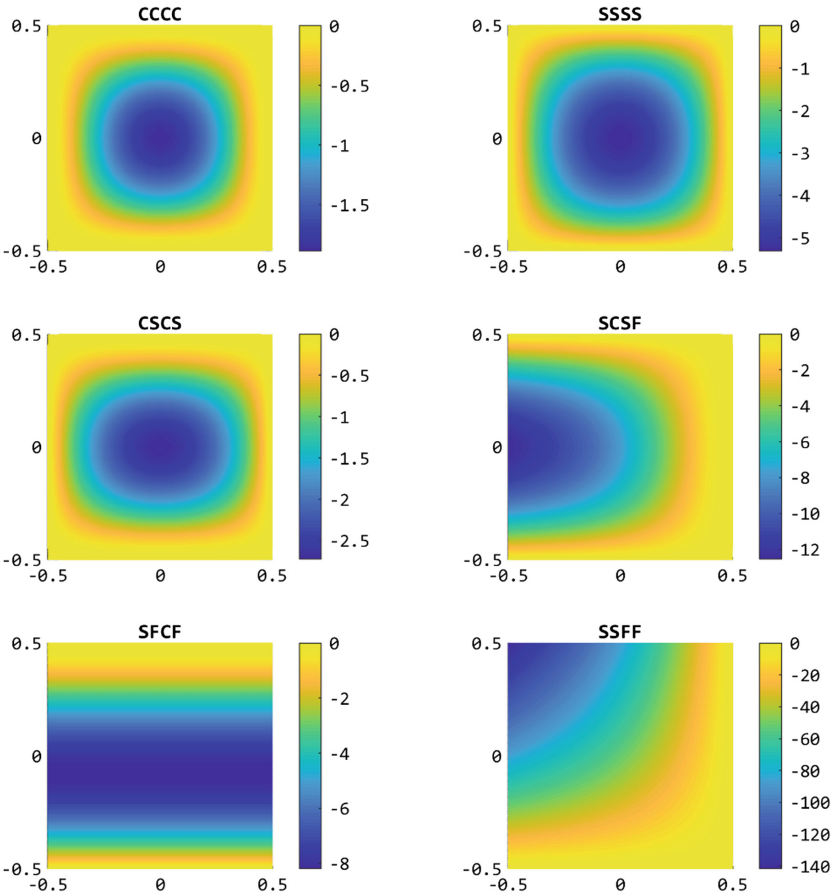

Fig. 4. The stress distribution (magnitude and direction) of fabric sheet yielded by the bending deformed under uniform pressure using 20 × 20 Q4 and one smoothing cell per element.

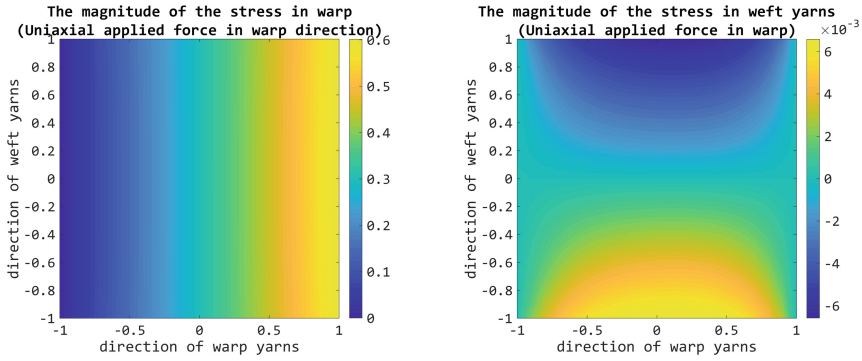

Fig. 5. The magnitude of the stress, under uniaxial applied force in warp direction, using 70 × 70 Q4 elements and one smoothing domains per element.

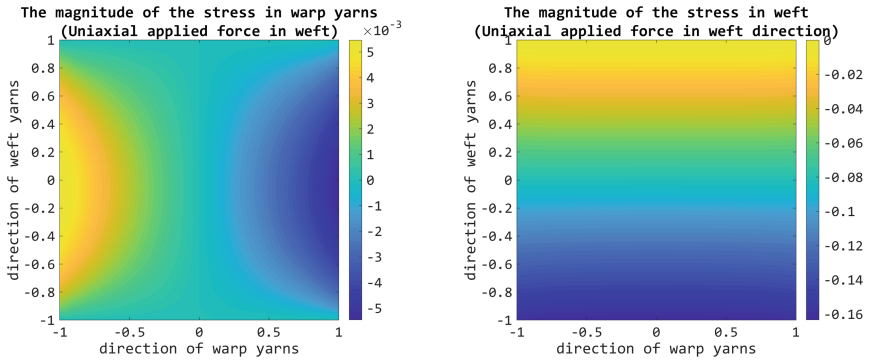

Fig. 6. The magnitude of the stress, under uniaxial applied force in weft direction, using 70 × 70 Q4 elements and one smoothing domains per element.

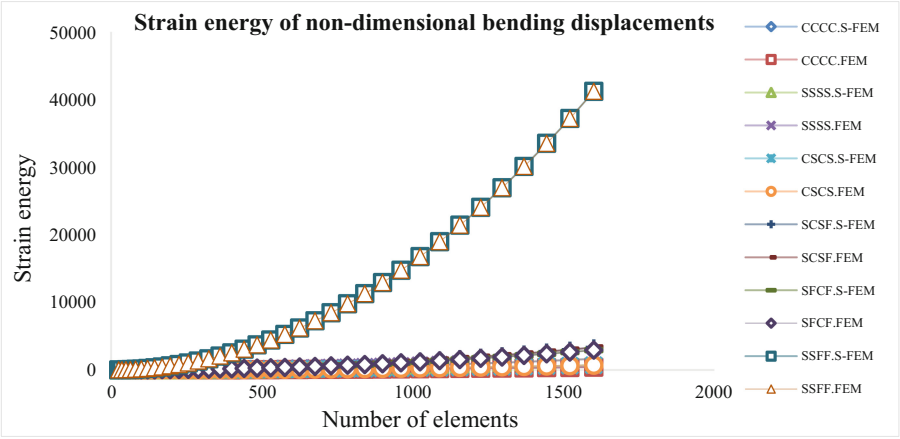

Fig. 7. Strain energy evaluated with FEM and CS-FEM for non-dimensional transverse displacements with different mesh density and boundary conditions subjected uniform load.

that the graphs of strain energy computed by CS-FEM model is approximate and coincided with that one of FEM on the same boundary conditions and mesh density under uniform pressure. However, the linear shape functions of CS-FEM using a point interpolation method (PIM) are constant as shown in Fig. 2. Vice versa, the shape functions of a Q4 element are those of bilinear Lagrange shape functions in natural coordinates $(\xi,\ \eta,\ \zeta)$ that are needed to be transformed into Cartesian coordinates $(x,\ y,\ z)$ when one evaluates strain gradient matrix. This requires a Jacobian transformation matrix and needs to be evaluated by one or more Gauss points. Thus, the strain smoothing technique reduces the computation time in terms of the central processing unit time.

6 Conclusions

The CS-FEM gives a higher computational efficiency in term of GPU time but effective performance in analyzing the bending and tensile behavior of woven fabric compared with standard FEM. Thus, the application of FOM and CS-FEM to displacement-based low-order finite element formulations, that based on quadrilateral plate/shell finite element models, are well refined and appropriate for numerical modelling and simulation of the mechanical deformation behavior of tensile and bending for woven fabric in terms of elastic material with both isotropy and orthotropic anisotropy.

Acknowledgments. The author (UMINHO/BPD/9/2017) and co-authors acknowledge the FCT funding from FCT – Foundation for Science and Technology within the scope of the project "PEST UID/CTM/00264; POCI-01-0145-FEDER-007136".

References

1. Koustoumpardis, P.N., Aspragathos, N.A.: Intelligent hierarchical robot control for sewing fabrics. Robot. Comput.-Integr. Manuf. **30**(1), 34–46 (2014)
2. Sengupta, S., Debnath, S., Sengupta, A.: Fabric bending behaviour testing instrument for technical textiles. Measurement **87**, 205–215 (2016)
3. Veit, D.: Simulation in Textile Technology: Theory and Applications. Woodhead Publishing Series in Textiles, 1st edn. Woodhead Publishing, Cambridge (2012)
4. Zhang, Y.T., Fu, Y.B.: A micro-mechanical model of woven fabric and its application to the analysis of buckling under uniaxial tension. Part 2: buckling analysis. Int. J. Eng. Sci. **39**(1), 1–13 (2001)
5. Fan, J., Yu, W., Hunter, L.: Clothing Appearance and Fit: Science and Technology. Woodhead Publishing Series in Textiles. Woodhead Publishing, Cambridge (2004)
6. Hu, J.: Fabric Testing. Woodhead Publishing Series in Textiles. Woodhead Publishing, Cambridge (2008)
7. Hu, J.: Structure and Mechanics of Woven Fabrics. Woodhead Publishing Series in Textiles. Woodhead Publishing, Cambridge (2004)
8. Chen, J.-S., et al.: A stabilized conforming nodal integration for Galerkin mesh-free methods. Int. J. Numer. Methods Eng. **50**(2), 435–466 (2001)
9. Liu, G.R., Zeng, W., Nguyen-Xuan, H.: Generalized stochastic cell-based smoothed finite element method (GS_CS-FEM) for solid mechanics. Finite Elem. Anal. Des. **63**, 51–61 (2013)
10. Yue, J., et al.: A cell-based smoothed finite element method for multi-body contact analysis using linear complementarity formulation. Int. J. Solids Struct. **141–142**, 110–126 (2018)
11. Feng, S.Z., Li, A.M.: Analysis of thermal and mechanical response in functionally graded cylinder using cell-based smoothed radial point interpolation method. Aerosp. Sci. Technol. **65**, 46–53 (2017)
12. Tootoonchi, A., et al.: A cell-based smoothed point interpolation method for flow-deformation analysis of saturated porous media. Comput. Geotech. **75**, 159–173 (2016)
13. Bathe, K.-J., Dvorkin, E.N.: A four-node plate bending element based on Mindlin/Reissner plate theory and a mixed interpolation. Int. J. Numer. Methods Eng. **21**(2), 367–383 (1985)
14. Duan, H., Ma, J.: Continuous finite element methods for Reissner-Mindlin plate problem. Acta Mathematica Scientia **38**(2), 450–470 (2018)

15. Wu, F., et al.: A generalized probabilistic edge-based smoothed finite element method for elastostatic analysis of Reissner-Mindlin plates. Appl. Math. Model. **53**, 333–352 (2018)
16. Thai-Hoang, C., et al.: A cell—based smoothed finite element method for free vibration and buckling analysis of shells. KSCE J. Civ. Eng. **15**(2), 347–361 (2011)
17. Liu, G.R., Dai, K.Y., Nguyen, T.T.: A smoothed finite element method for mechanics problems. Comput. Mech. **39**(6), 859–877 (2007)
18. Nguyen-Xuan, H., et al.: A node-based smoothed finite element method with stabilized discrete shear gap technique for analysis of Reissner-Mindlin plates. Comput. Mech. **46**(5), 679–701 (2010)